Chapter 2

Mechanical Properties of Weld Deposits

Many engineering components are fabricated using welding. The integrity of the fabrication is usually asserted on the basis of mechanical properties. Strength, ductility and toughness are considered as the essential mechanical properties. Previous work on the modelling of weld metal mechanical properties is reviewed in this Chapter.

2.1 Strength

The capacity of a material to withstand static load can be determined using a tensile test, in which a standard specimen is subjected to a continually increasing uniaxial load until it fractures, Fig. 2.1. The load–elongation curve is plotted and the results are usually restated in terms of stress and strain, which within reasonable limits are independent of the geometry of specimen, Fig. 2.2a:

$$\text{Engineering stress, } \sigma_E = \frac{P}{A_0} \tag{2.1}$$

$$\text{Engineering strain, } \epsilon_E = \frac{L_f - L_0}{L_0} \tag{2.2}$$

where P is the load, A_0 is initial cross–sectional area and L_0 and L_f are initial and final lengths of the sample respectively.

The material at first extends elastically; if the load is released the sample returns to its original length. After exceeding the elastic limit the deformation is said to be plastic, so the sample does not regain its original length if the load is released. With continued loading the engineering stress reaches a maximum beyond which the sample develops a neck. This local decrease in cross-sectional area focuses deformation until the sample fractures.

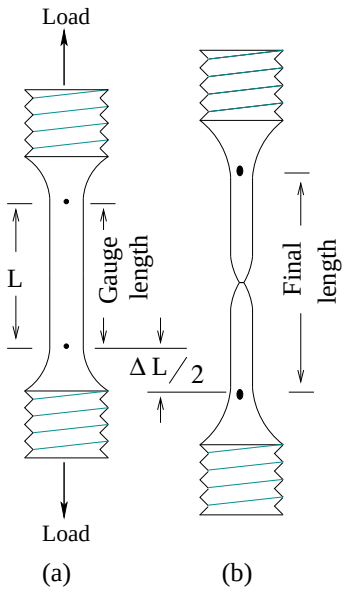

Figure 2.1: Schematic diagram of tensile test specimen, a) before testing b) after testing. $\triangle$ L is the total extension of the specimen during the tensile test.

The yield stress is defined as the stress at which plastic deformation just starts as the stress–strain curve deviates from linearity. Because of the difficulty in precisely measuring this deviation, a '0.2% proof stress' is used which is the stress at 0.002 plastic strain, Fig. 2.2b. The proof stress is sometimes referred as the 'yield stress'. The maximum engineering stress is called the 'ultimate tensile stress', whereas the stress at which the sample fractures is called the 'fracture stress'.

Engineering stresses and strains do not account for the change in the load bearing cross–sectional area of the sample during deformation. The true stress and strain do so and are defined as follows:

$$\sigma = \sigma_E(\epsilon_E + 1) \tag{2.3}$$

$$\epsilon = \ln(\epsilon_E + 1) \tag{2.4}$$

This leads to a change in the form of the stress–strain plot as illustrated in Fig. 2.3.

The engineering strain and true strain are comparable at small strains. The flow curve of many metals as expressed in terms of the true stress σ and true strain ϵ can be represented as:

$$\sigma = K\epsilon^n \tag{2.5}$$

where 'K' is value of flow stress at ϵ=1.0 and 'n' is the strain hardening exponent. Both these

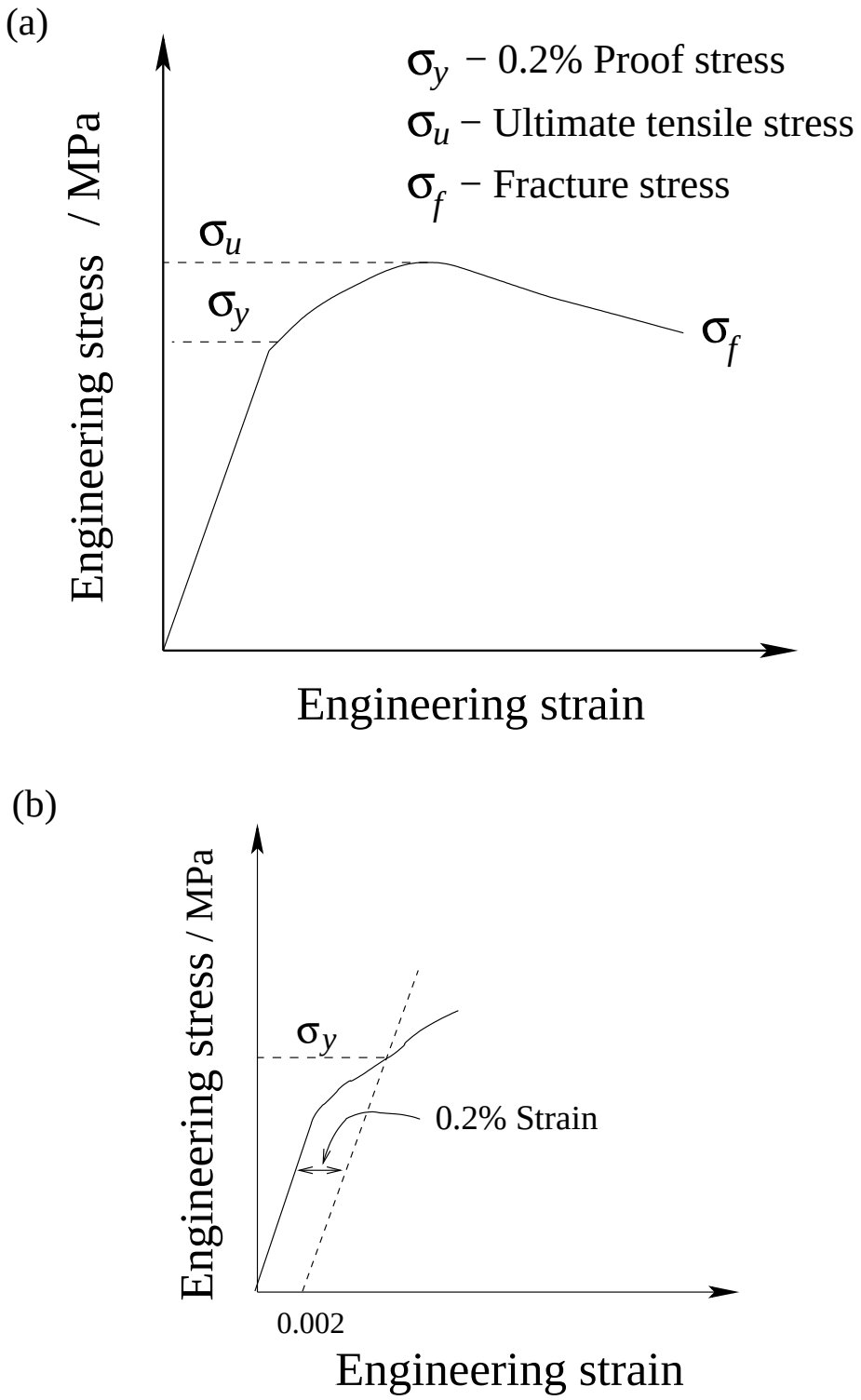

Figure 2.2: Engineering stress-strain curve showing a) different stresses, b) 0.2% proof stress.

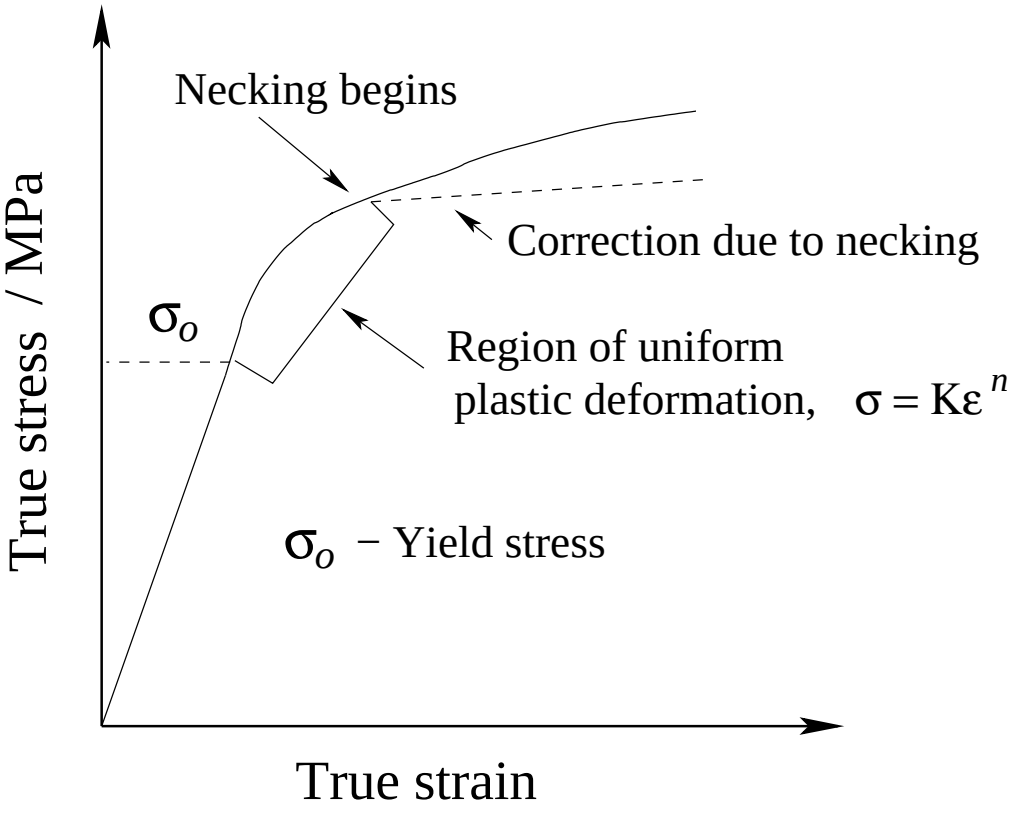

Figure 2.3: True stress - true strain curve (flow curve).

parameters can be estimated from a logarithmic plot of true stress and true strain. In practice, the strain hardening exponent may vary with strain but equation 2.5 is nevertheless a useful representation of plastic deformation.

2.2 Ductility

Ductility is important because an engineering component should show considerable plasticity before fracture. Ductility, as measured in a tensile test, is usually expressed as elongation or reduction in area:

$$\text{Elongation} = \frac{L_f - L}{L} \tag{2.6}$$

$$\text{Reduction in area} = \frac{A_f - A_0}{A_0} \tag{2.7}$$

where, L_f is the length of sample at fracture, L is initial length, A_0 is the initial area of cross-section and A_f is the area of cross–section at fracture. Both elongation and reduction in area

are frequently expressed as percentages.

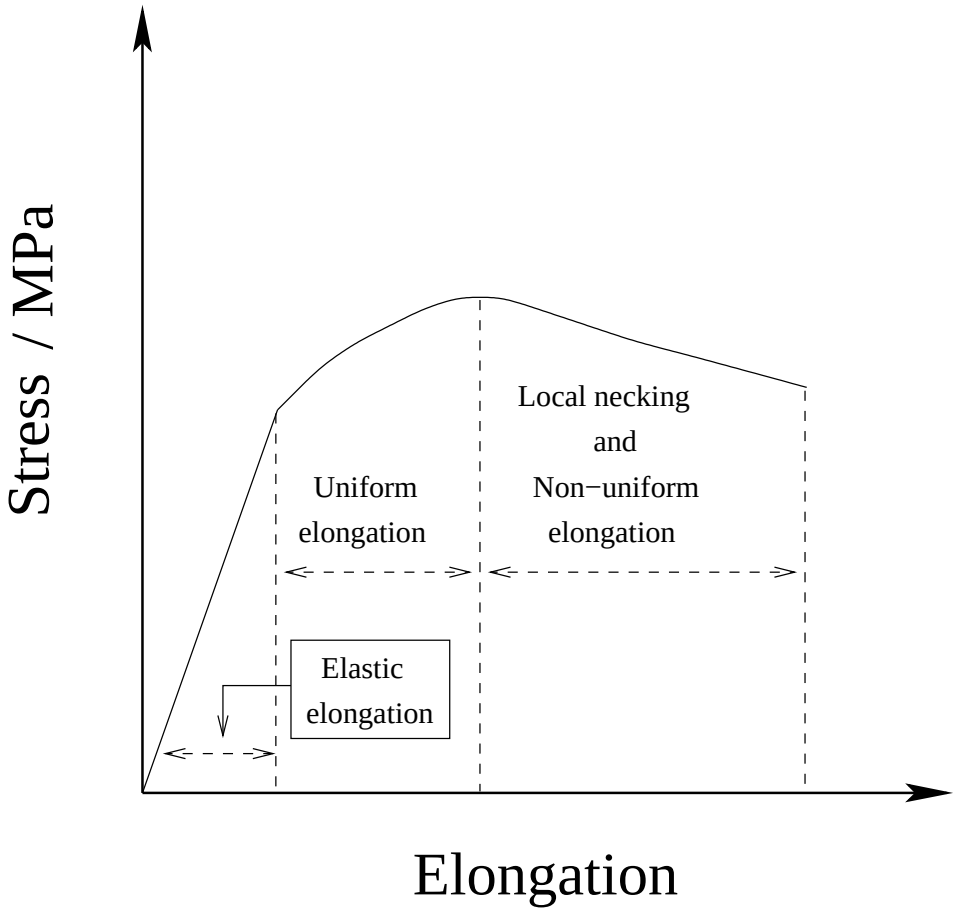

Figure 2.4: The stress-elongation curve. The elastic elongation is exaggerated for clarity.

Plastic strain can be subdivided into two components, an initial uniform strain where the cross–section of the sample is identical along the entire gauge length, and a non–uniform component beginning with the onset of necking. Assuming that equation 2.5 is a true representation of deformation, the stress at the point where necking begins is given by $\sigma = Kn^n$ [17].

2.3 Charpy Impact Toughness

Toughness is the ability of the material to absorb energy during the process of fracture. The ability to withstand occasional stresses above yield stress without fracturing is particularly desirable in engineering components. The welded joints should resist brittle fracture; therefore, the weld metal should be tough, with a great deal of energy being absorbed during the process of fracture. One of the popular test methods to characterise toughness is the Charpy impact

toughness test in which a square sectioned, notched sample (Fig. 2.5a) is fractured under specified conditions [18]. The absorbed energy during fracture is taken as a measure of toughness. However, Charpy impact test values are empirical since these results cannot be used directly in engineering design and can be used only to rank samples in research and development experiments. The test is usually conducted on a material over a range of temperatures to reveal any ductile–brittle transition, Fig. 2.5b.

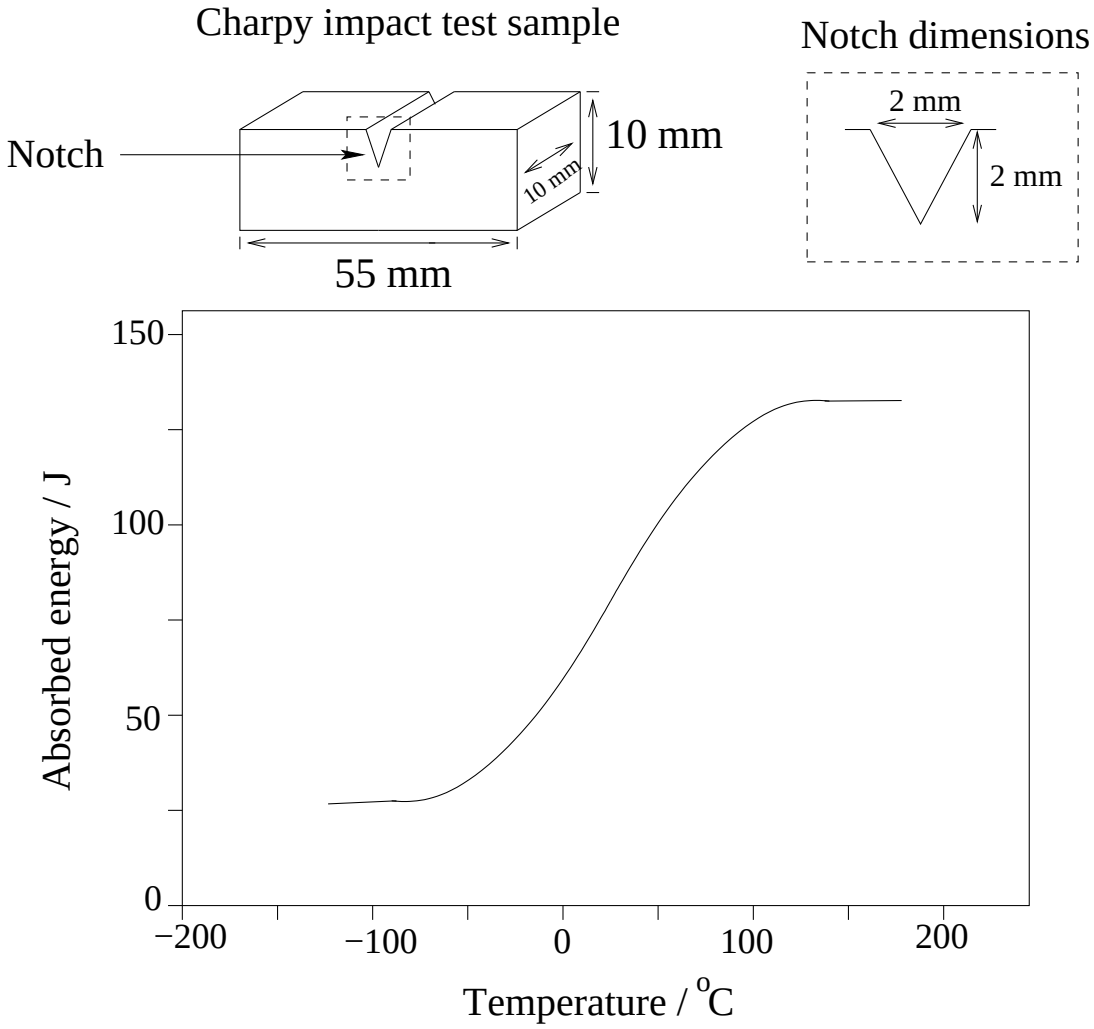

Figure 2.5: The Charpy impact test sample and impact toughness versus test temperature curve.

2.4 Strengthening Mechanisms

Iron in its pure form is weak and can have a yield strength as low as 50 MPa [19]. The strength of pure body–centered cubic iron in a fully annealed condition decreases rapidly as the temperature

is increased, Fig. 2.6. The strength is particularly sensitive to temperatures below -25 °C. In fact, it is this sensitivity to temperature which gives rise to the ductile–brittle transition. The cleavage strength of iron, is insensitive to temperature; at sufficiently low temperature it becomes less than the flow stress, making iron brittle.

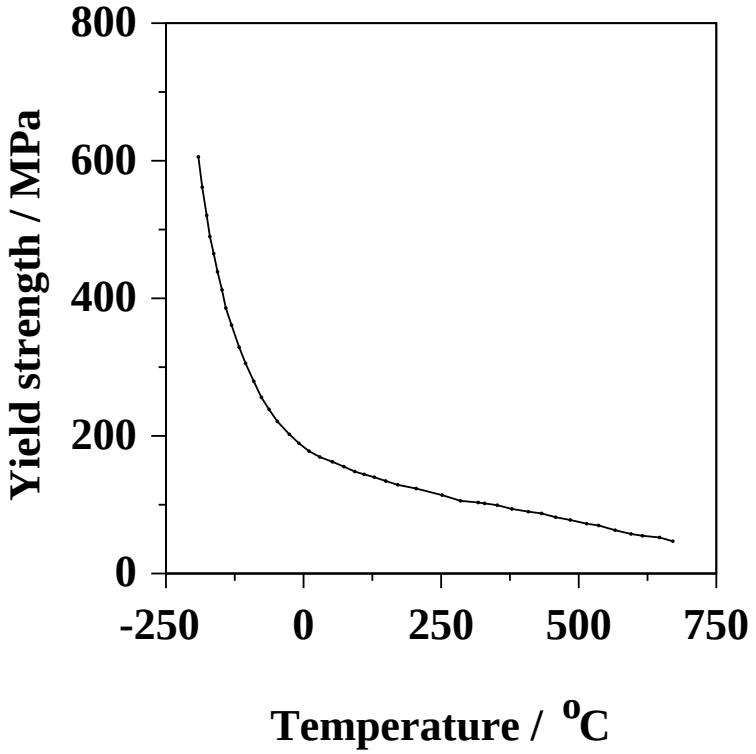

Figure 2.6: Temperature dependence of the yield strength of iron (gettered with titanium) at a plastic strain of 0.002 [12]. The strain rate is $2.5 \times 10^{-4}\ s^{-1}$.

2.4.1 Grain Refinement

The refinement of grain size leads not only to an increase in the strength but also toughness [20]. Grain boundaries are formidable obstacles to the movement of dislocations. The dependence of the yield strength on grain size is given by the Hall–Petch relationship [21]:

$$\sigma_y = \sigma_i + k_y d^{-1/2} \tag{2.8}$$

where 'd' grain diameter, σ_y is the yield stress, σ_i is the friction stress opposing the movement of dislocation in the grains and k_y is a constant.

The derivation of the Hall–Petch equation relies on the formation of a dislocation pile–up at a grain boundary, one which is large enough to trigger dislocation activity in an adjacent grain. Yield in a polycrystalline material is in this context defined as the transfer of slip across grains.

A larger grain is able to accommodate more dislocations in a pile–up, enabling a larger stress concentration at the boundary, thereby making it easier to promote slip in the nearby grain [22].

It is harder to propose a general mechanism by which grain refinement improves toughness. The argument for steels is that grain boundary cementite particles are finer when the grain size is small [22]. Fine particles are more difficult to crack and any resulting small cracks are difficult to propagate, thus leading to an improvement in toughness.

2.4.2 Solid Solution Hardening

The most common method of increasing the hardness and strength of steels is by solid solution strengthening. The degree of hardening or softening due to dissolved elements depends crudely on the relative difference in atomic size relative to an iron atom [12]. Large atoms induce compressive stress fields whereas smaller atoms are associated with tensile fields in the matrix. These distortion interact with dislocation motion. Solid solution strengthening also depends on disturbances to the electronic structure, expressed in terms of the difference of the solute and host atom [20].

In steels the smaller atoms carbon and nitrogen occupy interstitial sites whereas elements like silicon, manganese are substitutional. The interstitial solute atoms cause an asymmetrical distortion of the ferrite lattice whereas the substitutional solute produce symmetrical distortions. Therefore the increase in strength of α–iron by interstitial carbon or nitrogen is much greater than that of any substitutional alloying element Fig. 2.7. Isotropic distortion can only interact with the hydrostatic stress fields of dislocations. Much greater interactions are possible with the tetragonal strains associated with the interstitial atoms in ferrite.

Fig. 2.8 shows that the strengthening due to substitutional solutes often goes through maximum as a function of temperature. In a few cases there is some softening in body centered cubic α–iron at low temperatures because the presence of foreign solute atom locally assists dislocations to overcome the large Peierls barrier to dislocation motion [1].

2.4.3 Precipitation Hardening

Small and uniformly distributed precipitates can be effective barriers to dislocation movement. Precipitation hardened steels strengthening are usually first heat treated in the austenite phase field in order to dissolve solutes and then cooled rapidly to ambient temperatures to produce a supersaturated ferrite or martensitic transformation. Tempering then allows the excess solute to precipitate as carbides or nitrides, thereby strengthening the microstructure. In steels the strong carbide–forming elements titanium, vanadium, niobium, molybdenum, *etc.* are commonly used as the main precipitation strengthening elements. This mechanism is applied widely to increase the creep strength of power plant steels.

2.5 Tempering

During welding, there are regions created which are austenitised and then cooled rapidly, producing brittle microstructures such as martensite. Tempering is frequently used to restore the toughness, by heat treating in a temperature regime where austenite cannot form.

Thus, any excess carbon in solution is rejected to form carbides. In some cases the purpose of tempering is to induce the precipitation of alloy carbides. Power plant steels containing carbide forming elements such Cr, Mo, V, Nb, Ti, and W form stable carbides such as MX, M_3X, M_2X, M_7X_3, $M_{23}X_6$ and M_6X (where M represents metal atoms, X represents interstitial atoms) on tempering at temperatures where there is sufficient mobility for the diffusion of substitutional atoms. This generally means temperatures above 500 °C. The precipitation of alloy carbides and the associated strengthening is often referred to as 'secondary hardening' [23]. Fig. 2.9 shows the variety of carbides formed during tempering of water quenched $2\frac{1}{4}$Cr–1Mo steel from its austenitisation temperature.

2.6 Previous Weld Mechanical Property Models

Weld metal models can in general be categorised into two classes, those which are empirical and others founded on physical metallurgy. The latter are more meaningful, but as will be seen later, they are generally over–simplified and deal only with simple properties rather than the range of properties important in engineering design.

2.6.1 Regression Models

There have been numerous attempts to model weld metal mechanical properties by using linear regression analysis (e.g. Table 2.1). The strength of weld metal is frequently modelled as a function of chemical composition of weld metal, for cases where all the remaining variables associated with welding approximately constant. Equations like these are useful within the context of the experiments they represent. Naturally, the form of the relationships used may not necessarily be justified in detail.

2.6.2 The Sugden–Bhadeshia Model

Sugden and Bhadeshia tried to predict the strength of the as–deposited weld as a function of the chemical composition and microstructure [25]. The model is based on the assumption that the strength can be factorised into components; strength of pure iron, solid solution strengthening and strength due to microstructure, equation 2.9. The chosen microstructural constituents are allotriomorphic ferrite (α), Widmanstätten ferrite (α_w) and acicular ferrite (α_a) with the following assumptions:

Carbon–Manganese	YS = 335 + 439 C + 60 Mn + 361 (C.Mn) UTS = 379 + 754 C + 63 Mn + 337 (C.Mn)
Silicon–Manganese	YS = 293 + 91 Mn + 228 Si - 122 Si^2 UTS = 365 + 89 Mn + 169 Si - 44 Si^2
Chromium–Manganese	YS = 320 + 113 Mn + 64 Cr + 42 (Mn.Cr) UTS = 395 + 107 Mn + 63 Cr + 36 (Mn.Cr)
Nickel–Manganese	YS = 332 + 99 Mn + 9 Ni + 21 (Mn.Ni) UTS = 401 + 102 Mn + 16 Cr + 15 (Mn.Ni)

Table 2.1: Yield and ultimate tensile strength (MPa) models developed using regression analysis for as–welded carbon–manganese weld metals [2]. The alloying element concentrations are expressed in wt%.

1) The total strength of as–welded deposit is assumed to be a linear combination of individual components:

$$\sigma_y = \sigma_{\text{Fe}} + \sum_{i=1}^{n} \sigma_{SS,i} + \sigma_{\text{Micro}} \tag{2.9}$$

where σ_{Fe} is the strength of fully annealed pure iron as a function of temperature and strain rate, $\sigma_{SS,i}$ is the solid solution strengthening due to alloying element i and σ_{Micro} is strengthening due to weld metal microstructure.

2) The weld microstructure consists of allotriomorphic ferrite (α), Widmanstätten ferrite (α_w) and acicular ferrite (α_a). The variation in the grain sizes of α, α_w and α_a are not taken into account:

$$\sigma_{\text{Micro}} = \sigma_\alpha \, V_\alpha + \sigma_a \, V_a + \sigma_w \, V_w \tag{2.10}$$

where σ_α, σ_w and σ_a denote the contributions from 100% allotriomorphic ferrite, Widmanstätten ferrite and acicular ferrite respectively, and V_α, V_w and V_a are their corresponding volume fractions.

3) Nitrogen is assumed to be in solid solution and any strain ageing effects in the as-welded microstructure are assumed to be negligible.

4) The solid solution strengthening (σ_{SS}) is expressed as the sum of the contributions from each solute:

$$\sigma_{SS} = a \text{ Mn wt\%} + b \text{ Si wt\%} + ... \tag{2.11}$$

where the coefficients *a, b, ..* are functions of temperature, defining the role of the respective alloying elements. The values for these coefficients are taken from the published experimental data which are based on studies in which solid solution strengthening is studied in isolation.

An alloying element naturally influences more than just solid solution effects. However, the other consequences are included in the analysis via incorporation of microstructure. The authors were able to estimate the strength of individual microstructures (σ_α, σ_a and σ_w) by studying three welds which are made with identical welding conditions [25]. The chemical compositions were adjusted to give different fractions of microstructure in order to deduce the strengthening due to each microstructure (α, α_a and α_w). The final form of developed equation is;

$$\sigma_y = \sigma_{\mathrm{Fe}} + \sigma_{SS} + 27V_\alpha + 402V_a + 486V_w \quad \text{(MPa)} \tag{2.12}$$

where σ_{Fe} and σ_{SS} can be obtained from referred published literature [25].

Although the Sugden–Bhadeshia model has more physical meaning when compared with the empirical equations presented in Table 2.1, the model still has linear approximations which are not justified in detail. It is restricted to structural steel welds which have simple, untempered microstructures; bainite and martensite are excluded from the analysis, as is precipitation hardening. Young and Bhadeshia have developed the work for microstructures which are mixtures of bainite and martensite but this model has yet to be applied to weld metal microstructures. The model is nevertheless discussed below because it is interesting.

2.6.3 The Young–Bhadeshia Model

The Young–Bhadeshia strength model for high–strength steels [4] considered microstructures which are mixtures of martensite and bainite;

$$\sigma = \sigma_{\mathrm{Fe}} + \sum_i \sigma_{SS,i} + \sigma_C + K_L(\overline{L})^{-1} + K_D\rho_D^{0.5} + K_p\triangle^{-1} \tag{2.13}$$

where K_L, K_D and K_p are constants, σ_C is the solid solution strengthening due to carbon, $\overline{L}$ is a measure of the ferrite plate width, ρ_D is the dislocation density and $\triangle$ is the distance between any carbide particles. The other terms have their usual meanings.

Carbon

The carbon concentration in bainitic ferrite is assumed as 0.03 wt%, unlike the martensite which is supersaturated. Thus, the strengthening effect of carbon at the low concentrations typical in

bainite takes the form;

$$\sigma_{SS_C} = 1722.5 \times x^{1/2} \qquad \text{(MPa)} \tag{2.14}$$

where x is the concentration of carbon in wt%. For martensite when the carbon concentration can be large, there is evidence [26] to show that;

$$\sigma_{SS_C} = 1171.3 \times x^{1/3} \qquad \text{(MPa)} \tag{2.15}$$

Dislocations

The bainite and martensite transformations are associated with a shape deformation which may be accommodated by plastic relaxation. This leads to accumulation of dislocations. The amount of plastic deformation and dynamic recovery depends on the transformation temperature, therefore the dislocation density ρ_D is taken as a function of temperature, equation 2.16.

$$\log_{10}\{\rho_D\} = 9.2840 + \frac{6880.73}{T} - \frac{1780360}{T^2} \tag{2.16}$$

where T is the temperature in Kelvin and ρ_D is in m^{-2}. Equation 2.16 is taken from data over 570–920 K and should not be extrapolated. For transformation temperatures below 570 K the dislocation density is considered to be that at 570 K. The strengthening due to dislocations is estimated as;

$$\begin{aligned} \sigma_\rho &= 0.38\ \mu b(\rho_D)^{0.5} \\ &\cong 7.34 \times 10^{-6}(\rho_D)^{0.5} \qquad \text{(MPa)} \end{aligned} \tag{2.17}$$

where μ is the shear modulus and b is the magnitude of the Burgers vector.

Lath Size

Bainite and martensite in low alloy steels occur in the form of fine plates or laths. Here the dislocation sources are found at grain boundaries which is different from the classical Hall–Petch effect which considers the dislocations sources within individual grains. The increase in strength due to plate size is given by;

$$\sigma_G \cong 115(\overline{L})^{-1} \tag{2.18}$$

where σ_G is in MPa and $\overline{L}$ is the mean linear intercept taken on random sections and at random angles to the length of any plate section.

Carbide Particles

The strengthening σ_θ due to a uniform dispersion of spherical carbides particles is considered to be;

$$\sigma_\theta \cong 0.52 V_\theta \triangle^{-1} \qquad \text{(MPa)} \tag{2.19}$$

where $\triangle$ is the particle spacing and V_θ is the volume fraction of cementite. Bainite that occurs in high–strength low–alloy steels has most of its carbon partitioned into the residual austenite where it remains in solid solution. Young and Bhadeshia considered that cementite precipitation does not make significant contribution to the strength, but the carbon rejected into the austenite is important via its effects on the solid solution strengthening of martensite which forms during the cooling of austenite to ambient temperature.

The Young and Bhadeshia model can be applied to estimate the strength of bainitic and martensitic welds by using rule of mixtures. Even though the model had considered the microstructural influence the model still built on the some of the assumptions made in Sugden and Bhadeshia model like linear summation effect of solid solution strengthening.

2.6.4 Neural Network Models

Neural networks are parameterised non–linear regression models which are discussed in detail in Chapter 3. Cool *et al.* had developed neural network models to predict the yield strength, ultimate tensile strength of weld metals as a function of chemical composition, welding parameters and heat treatment [27]. Around 1652 individual experimental data were used in the analysis.

2.7 Conclusions

The basic strengthening mechanisms in steels related to weld metal mechanical properties have been reviewed and discussed. There has been substantial progress in understanding the origins of the yield strength of sample weld metal microstructure of allotriomorphic ferrite, Widmanstätten ferrite and acicular ferrite. Similar progress seems unlikely for those mechanical properties such as the ultimate tensile strength, ductility and toughness, all of which involve gross plasticity. Another difficulty is that the effects of heat treatments are not included explicitly in any mechanical property models.

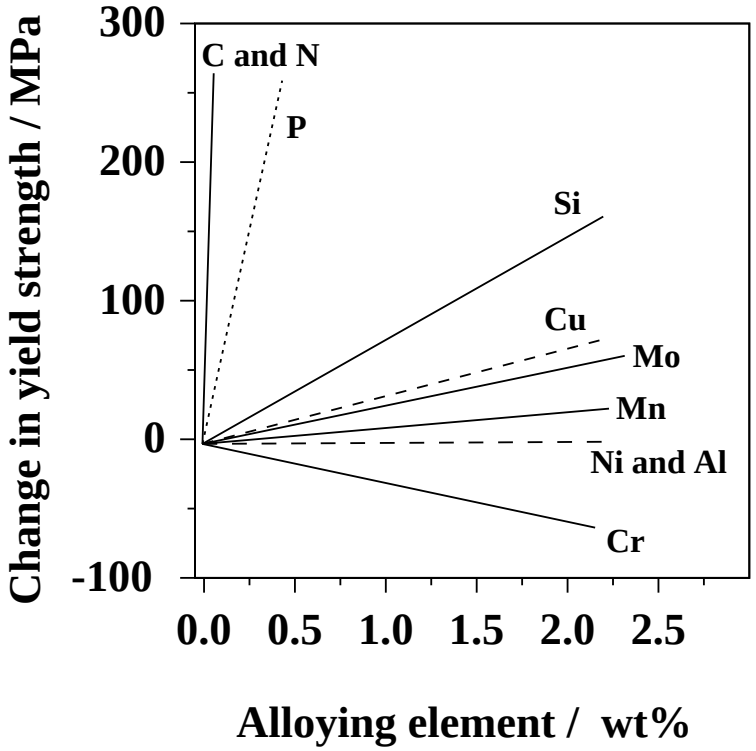

Figure 2.7: Contributions to the solid solution strengthening of ferrite [20].

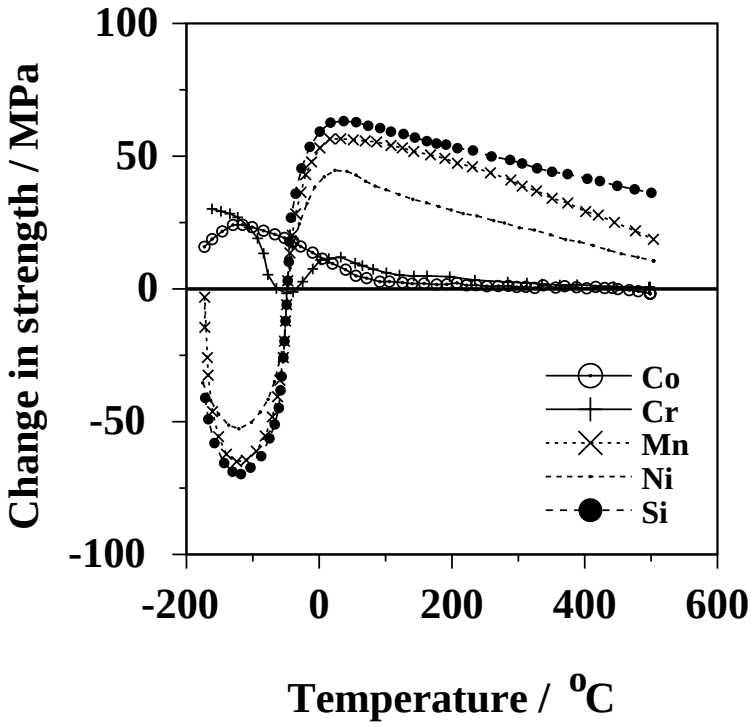

Figure 2.8: The effect of some substitutional solutes (3 at.%) on the yield strength of iron [12]. The strain rate is $2.5\times10^{-4}\ s^{-1}$.

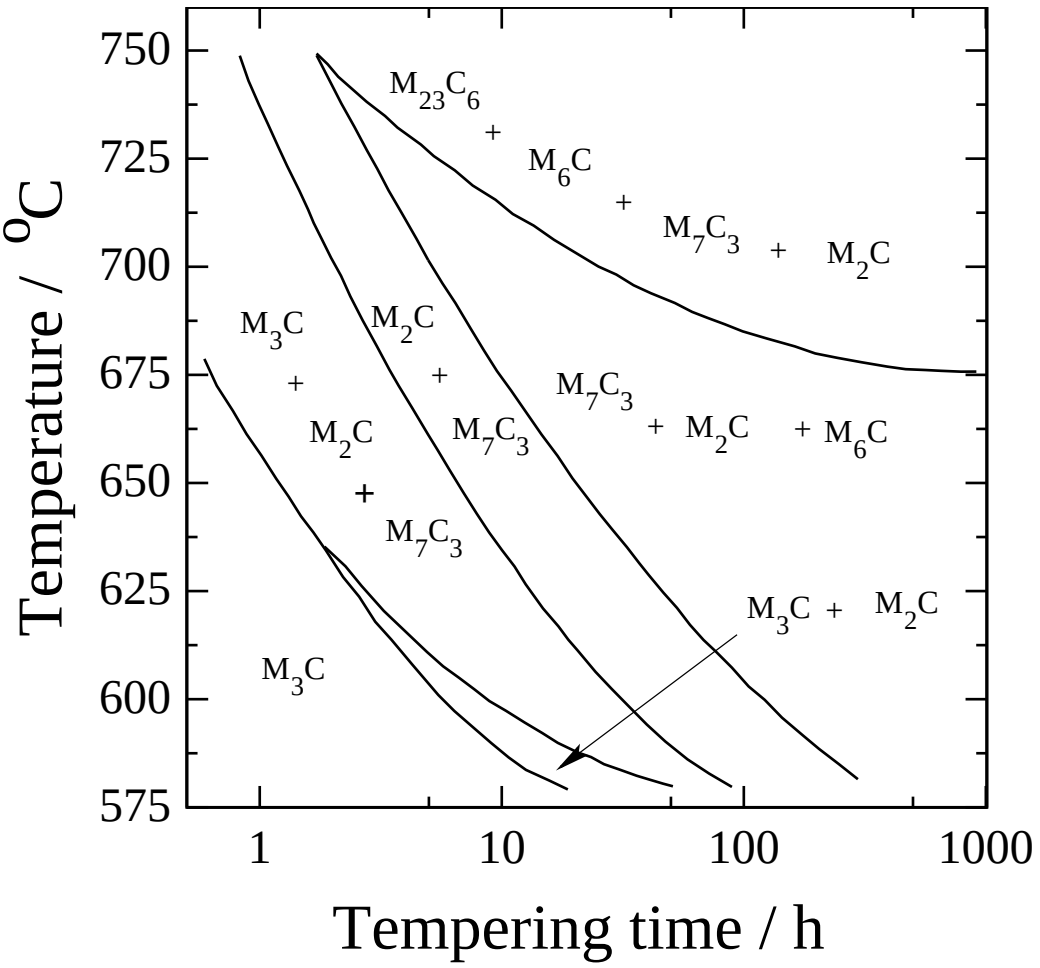

Figure 2.9: Carbide sequence in water quenched $2\frac{1}{4}$Cr–1Mo steel [24], where 'M' represents metallic elements.